Supplementary Material

Regulating reaction intermediates adsorption via electronic structural engineering of MoN/Co_4N for efficient water splitting

Yu Wang[a], Yaxiao Cui[a], Xueyi Zhao[a], Xiaodan Xia[a], Wenhui Li[a], Zexing Wu[a], Yanru Liu[a]*, Volodymyr Turkevych[b], Lei Wang[a]*

[a] Key Laboratory of Eco-chemical Engineering, Ministry of Education, International Science and Technology Cooperation Base of Eco-chemical Engineering and Green Manufacturing, College of Chemistry and Molecular Engineering, Qingdao University of Science & Technology, 53 Zhengzhou Road, 266042, Qingdao, P. R. China

[b] V. Bakul Institute for Superhard Materials, National Academy of Sciences of Ukraine, Kyiv 04074, Ukraine

* E-mail: liuyanru@qust.edu.cn (Yanru Liu), inorchemwl@126.com (Lei Wang).

1. Experimental section

1.1 Chemicals and materials

$Co(NO_3)_2·6H_2O$ (98%) was purchased from the official website of Shanghai Adamas Reagent Co., Ltd. Dimethylimidazole (2-MI) and $C_{10}H_{14}MoO_6$ were purchased from Maclean's Biochemical Technology Ltd (Shanghai, China). Ethanol and methanol purchased from Sinopharm Chemical Reagent Co. Commercially available platinum on activated carbon (20 wt% Pt/C) and Nafion (5 wt%) were purchased from Sigma-Aldrich. All chemicals were used as received without further purification.

1.2 Materials synthesis

Synthesis of ZIF-67: Dissolve 0.292 g of $Co(NO_3)_2·6H_2O$ and 0.658 g of 2-MI in 20 ml of ethanol, stirring at room temperature for 30 min. Afterward, pour Co^{2+} into a 2-MI solution and stir at room temperature for 1 hour. Afterward, centrifugation was performed, washed 3 times with anhydrous ethanol, and finally dried for 12 hours in a vacuum drying oven at 60 ℃.

Synthesis of MoCo@HZIF: 100 mg of ZIF-67 was dispersed in 15 ml of N,N-dimethylformamide (DMF), followed by 50 mg of molybdenum acetylacetonate ($C_{10}H_{14}MoO_6$) added to the solution and sonicated for 10 min. Transferred to a reactor and hydrothermally reacted at 150 °C for 6 hours. Cooled to room temperature, separated by centrifugation, washed three times with methanol and dried under vacuum at 60 °C to give MoCo@HZIF.

Synthesis of MoN/Co_4N@NC: To prepare the MoN/Co_4N@NC catalyst, the MoCo@HZIF precursor was heated to 500 °C in a tube furnace at a rate of 5 °C/min, held under a flowing ammonia atmosphere for 2 hours, and then naturally cooled to room temperature to obtain the sample.

Synthesis of Co_4N@NC, MoN/Co_4N@NC-0.25, MoN/Co_4N@NC-0.75 and MoN/Co_4N@NC-1: In the synthesis of precursors, the amount of Mo source added was adjusted to be 0 mg, 25 mg, 75 mg and 100 mg, respectively, and the other preparation procedures were the same as that of MoN/Co_4N@NC.

Synthesis of MoN@NC: The synthetic method was similar to that of MoN/Co_4N@NC, except that ZIF-67 was replaced with ZIF-8. The synthesis of ZIF-8 was performed according to a previously reported procedure[1].

1.3 Materials characterization

We detected the crystal structure and composition of the samples by testing X-ray diffraction (XRD) on X'Pert PRO MPD at a rate of 5 °C/min. The SEM and TEM investigations were conducted to observe the morphology of different samples on JEOL, JSM-7500F, and FEI, Tecnai-C20, respectively. In addition, the FEI, Tecnai-C20 was also used to further characterize the distribution and composition of samples by TEM-mapping and EDX testing. To characterize the surface chemical state of samples, we performed the X-ray photoelectron spectroscopy (XPS) on Thermo Scientific Escalab 250Xi.

1.4 Electrochemical measurement

For the preparation of the working electrode, 5 mg of the catalyst was dispersed in 1 mL of water/isopropanol (1:3 volume ratio) solvent followed by adding 25 μL of Nafion. After sonication for 30 min to form a homogeneous ink, a 10 μL drop was cast on a freshly polished RDGCE/GCE and dried under ambient conditions.

All electrochemical performance tests were conducted using an electrochemical workstation named Gamry Instruments Reference 3000. Typically, graphite rods, solid Ag/AgCl electrode, and glassy carbon electrode (GCE, 3 mm in diameter) were used as auxiliary, reference, and working electrodes in 1 M KOH, 0.5 M H_2SO_4, and 1 M PBS solution, respectively. Here, the potentials are given versus the reversible hydrogen electrode (RHE), transformed by the equation

$$\text{In 1.0 M KOH, } E_{RHE} = E_{SCE} + 1.068 \text{ V.}$$

Tafel slopes were deduced by fitting the corresponding LSV curves of overpotential vs log (j)

$$\eta = a + b \log j$$

Where η refers to the overpotential, b represents the Tafel slope, and j is the current density. Electrochemical impedance spectroscopy (EIS) was performed in a frequency window of 0.001 to 100000 Hz with a 5.0 mV amplitude. For the HER, the applied potential for EIS measurements was set at -1.219 V, and 0.393 V for the OER. The electrochemical double-layer capacitance (C_{dl}) was determined by the CVs performed in the non-Faraday process area. C_{dl} is the electric double-layer capacitance calculated from the non-Faradaic region and Cs is the specific capacitance of a flat, smooth electrode surface, whose value was numerically taken as 40 μF cm^{-2}.

$$ECSA = \frac{C_{dl}}{C_s}$$

1.5 DFT computation details

We performed the first-principles calculations in the frame of density functional theory (DFT) with the Vienna ab initio simulation package (VASP)[2]. The exchange-correlation energy is described by the Perdew-Burke-Ernzerhof (PBE) form of generalized-gradient approximation (GGA) exchange-correlation energy functional [3,4]. The structure optimizations of MoN and Co_4N have been carried out by allowing all atomic positions to vary and relaxing lattice parameters until the energy difference of successive atom configurations was less than 10^{-6} eV. The force on each atom in the relaxed structures was less than 0.015 eV/Å. The cutoff energy for the plane-wave basis set was set to 400 eV. The k-point spacing was set to be smaller than 0.03 $Å^{-1}$ over Brillouin zone (BZ)[5].

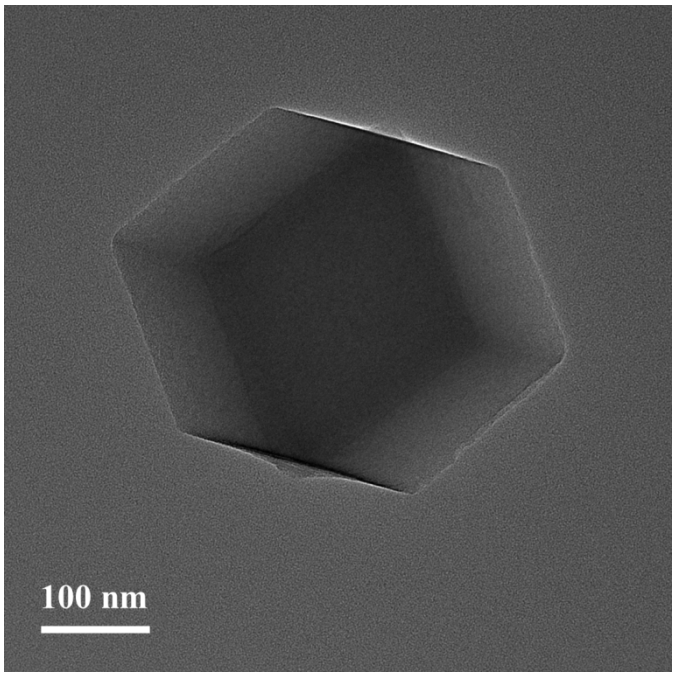

Figure S1. TEM image of ZIF-67.

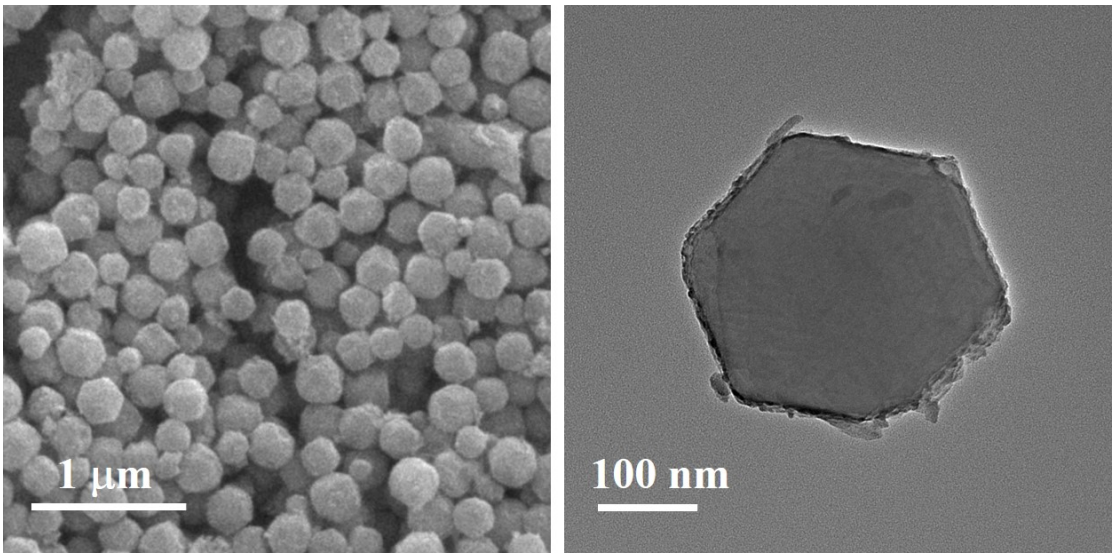

Figure S2. (a) SEM and (b) TEM images of MoCo@HZIF.

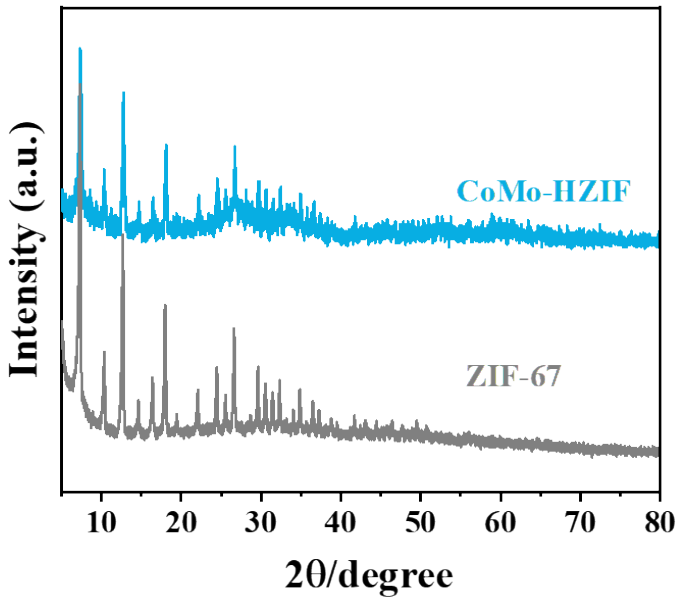

Figure S3. Simulation card of ZIF-67 and XRD pattern of CoMo-HZIF.

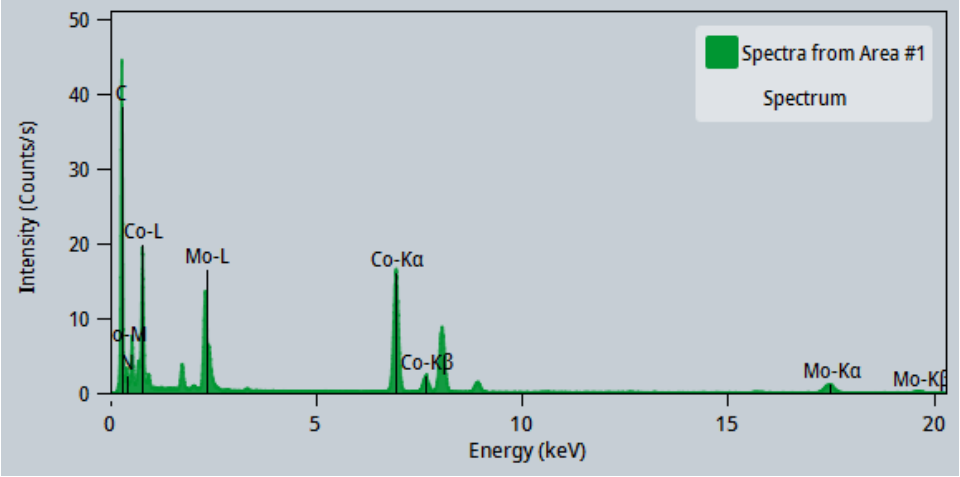

Figure S4. The EDS spectrum of MoN/Co_4N@NC.

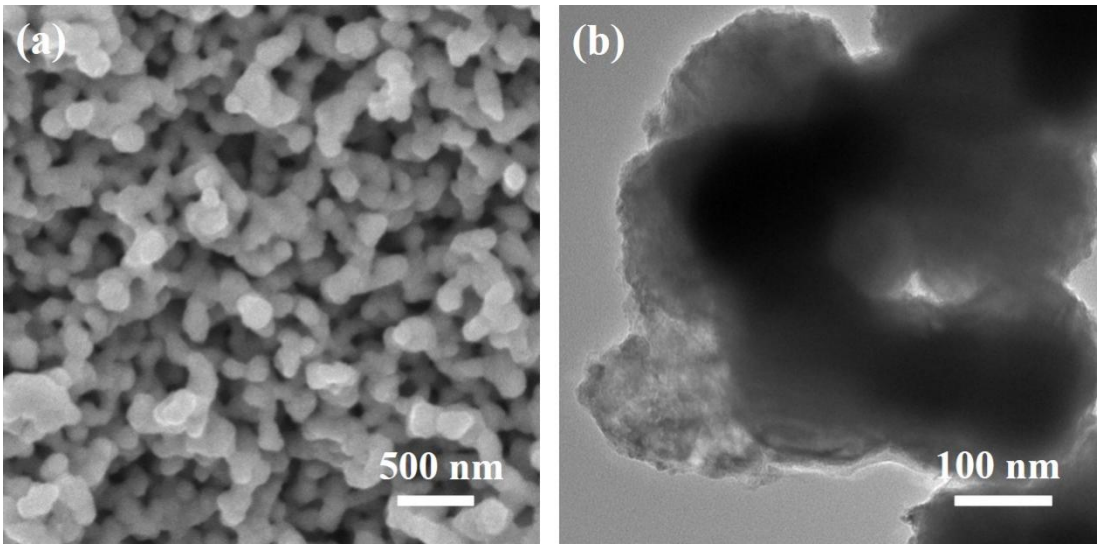

Figure S5. (a) SEM and (b) TEM images of Co_4N@NC.

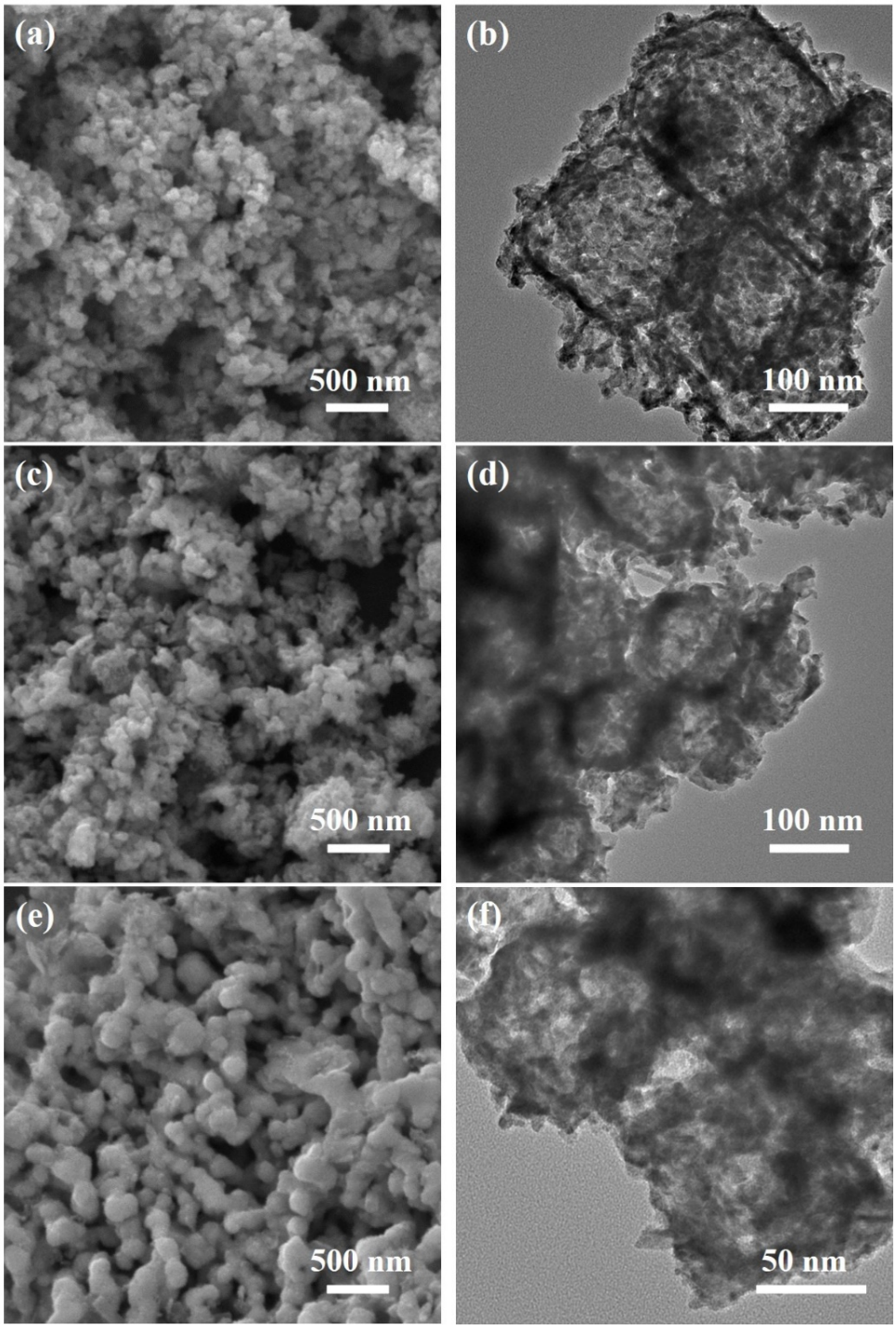

Figure S6. SEM images of samples MoN/Co_4N@NC-0.25, MoN/Co_4N@NC-0.75 and MoN/Co_4N@NC-1 are (a), (b) and (c), respectively.

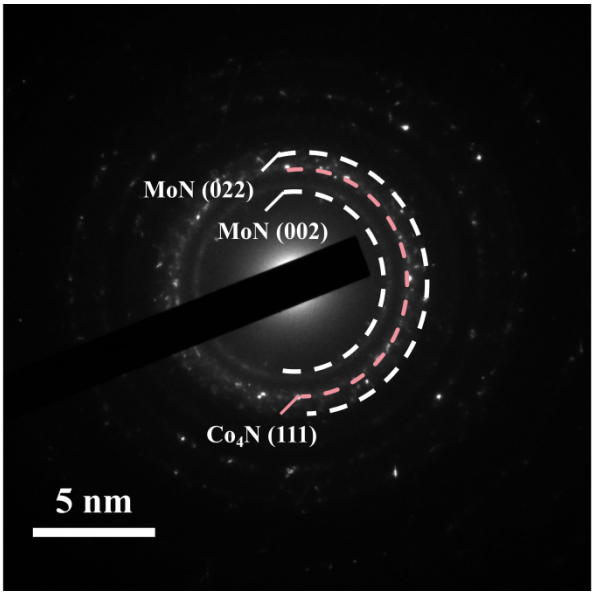

Figure S7. SAED patterns of MoN/Co_4N@NC.

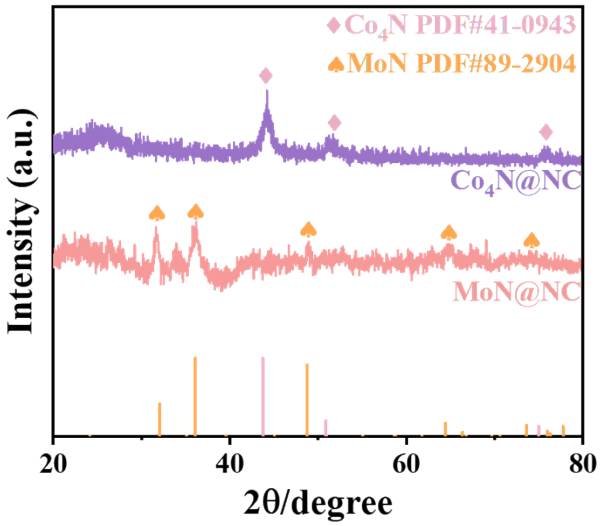

93

94 **Figure S8.** XRD patterns of (a) Co_4N@NC and (b) MoN@NC.

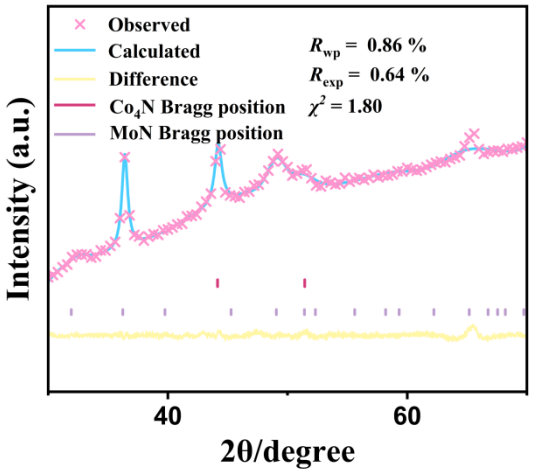

Figure S9. Rietveld refinement pattern of MoN/Co_4N@NC.

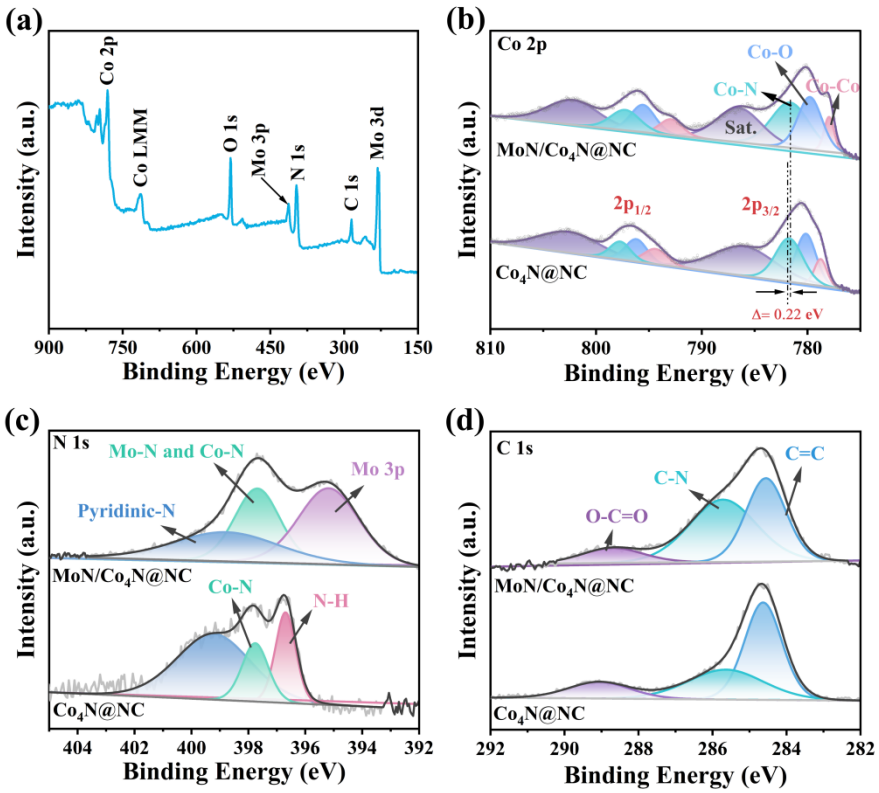

Figure S10. (a) XPS survey spectra of MoN/Co_4N@NC. High-resolution XPS spectra of (b) Co 2p, (c) N 1s and (d) C 1s for MoN/Co_4N@NC and Co_4N@NC.

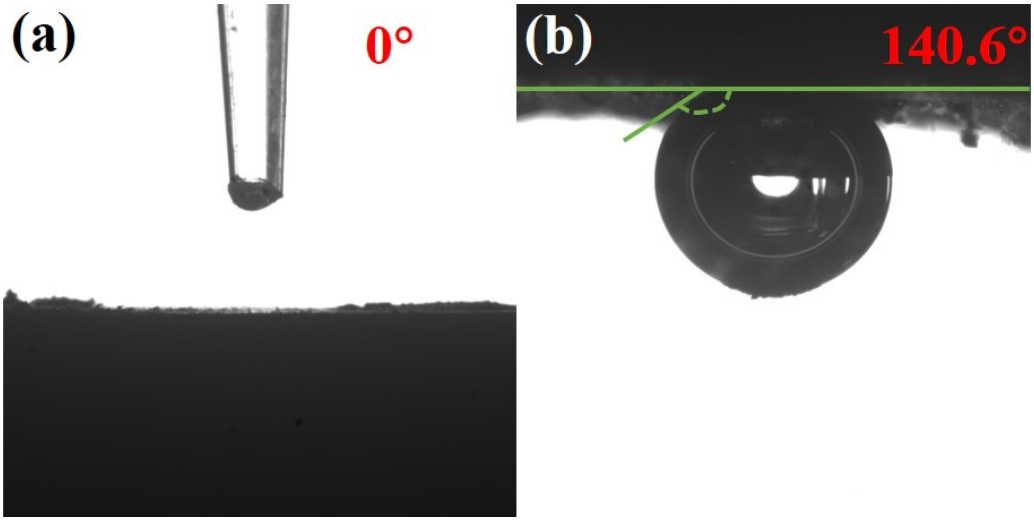

Figure S11. (a) and (b) are images of the water and bubble contact angles for MoN/Co_4N@NC, respectively.

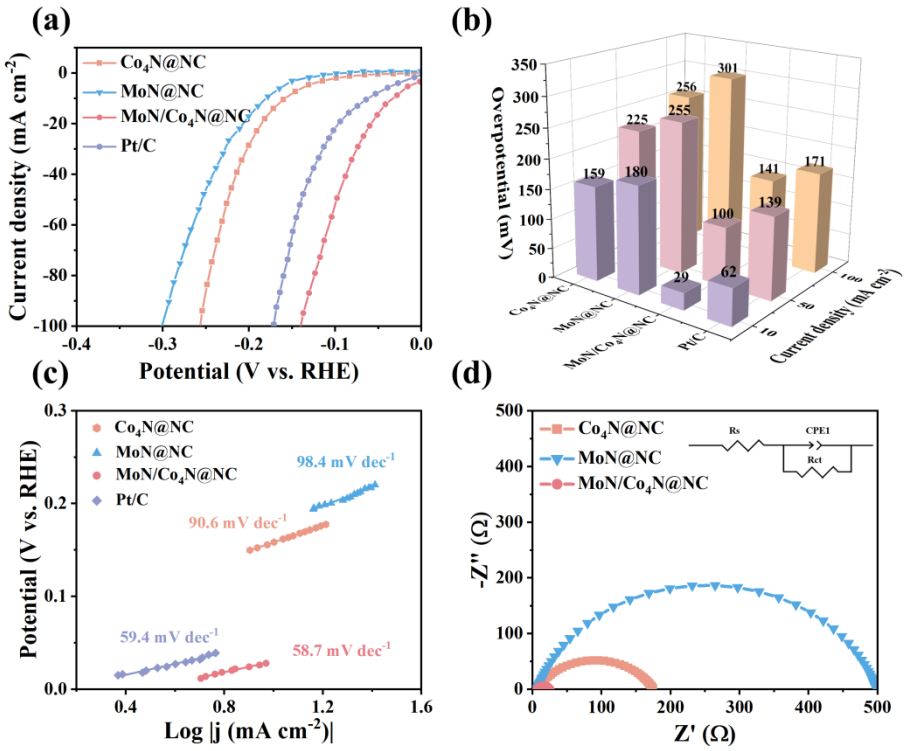

104

105 **Figure S12.** (a) LSV polarization curves and (b) overpotentials at 10, 50, and 100 mA cm^{-2} of

106 Co_4N@NC, MoN@NC, MoN/Co_4N@NC and Pt/C. (c) Tafel plots for Co_4N@NC, MoN@NC,

107 MoN/Co_4N@NC and Pt/C. (d) Electrochemical impedance spectra of the Co_4N@NC, MoN@NC

108 and MoN/Co_4N@NC.

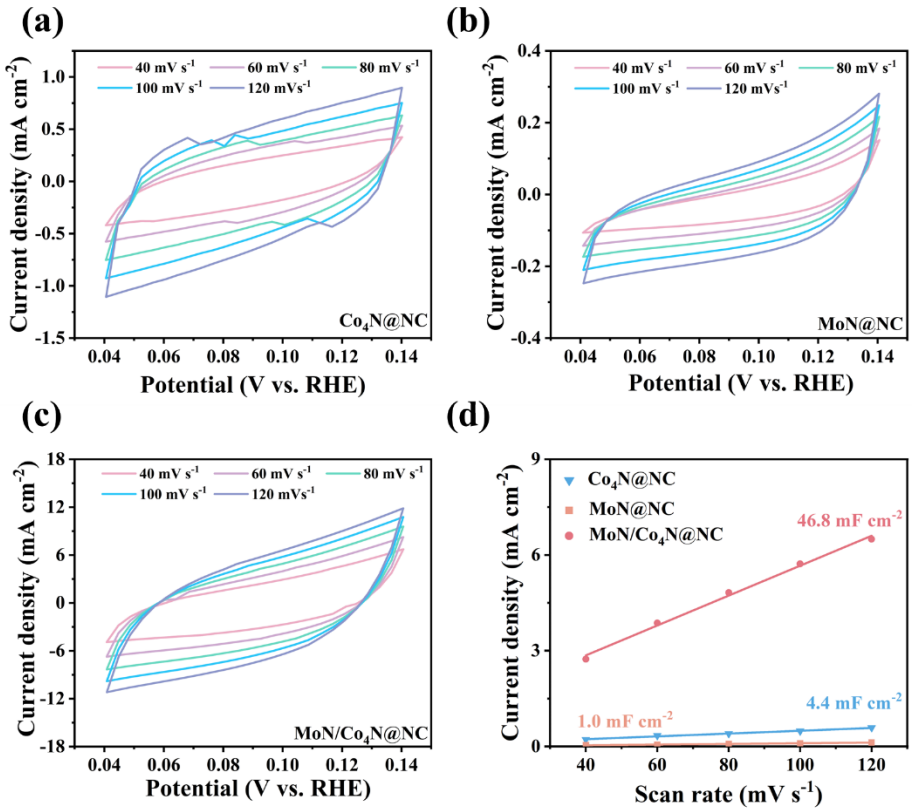

Figure S13. CV curves of (a) Co_4N@NC, (b) MoN@NC and (c) MoN/Co_4N@NC in the potential range of 0.04~0.14 V *vs.* RHE at various CV scan rates (40~120 mV s^{-1}) in 1.0 M KOH. (d) Double-layer capacitance (C_{dl}).

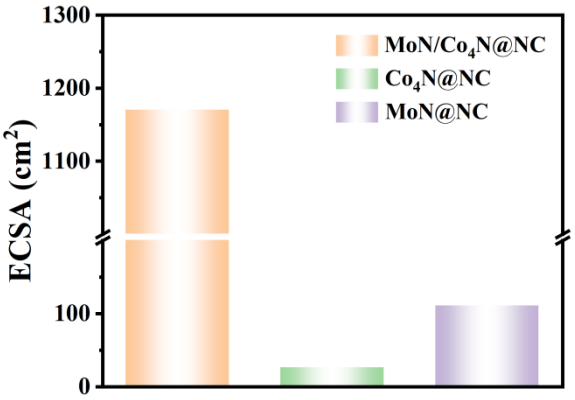

Figure S14. ECSA values of Co_4N@NC, MoN@NC, MoN/Co_4N@NC in 1 M KOH media for HER.

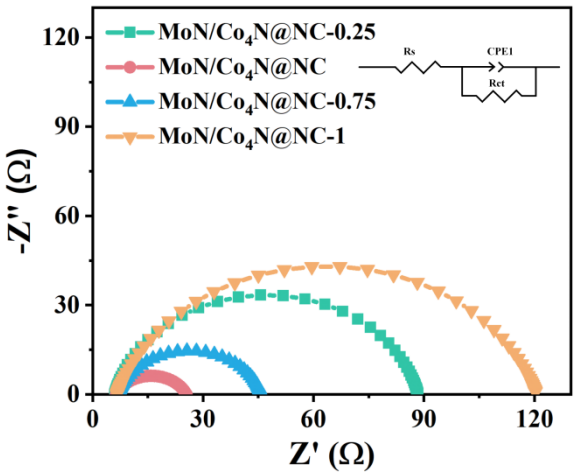

Figure S15. Electrochemical impedance spectra of the MoN/Co_4N@NC-0.25, MoN/Co_4N@NC, MoN/Co_4N@NC-0.75 and MoN/Co_4N@NC-1.

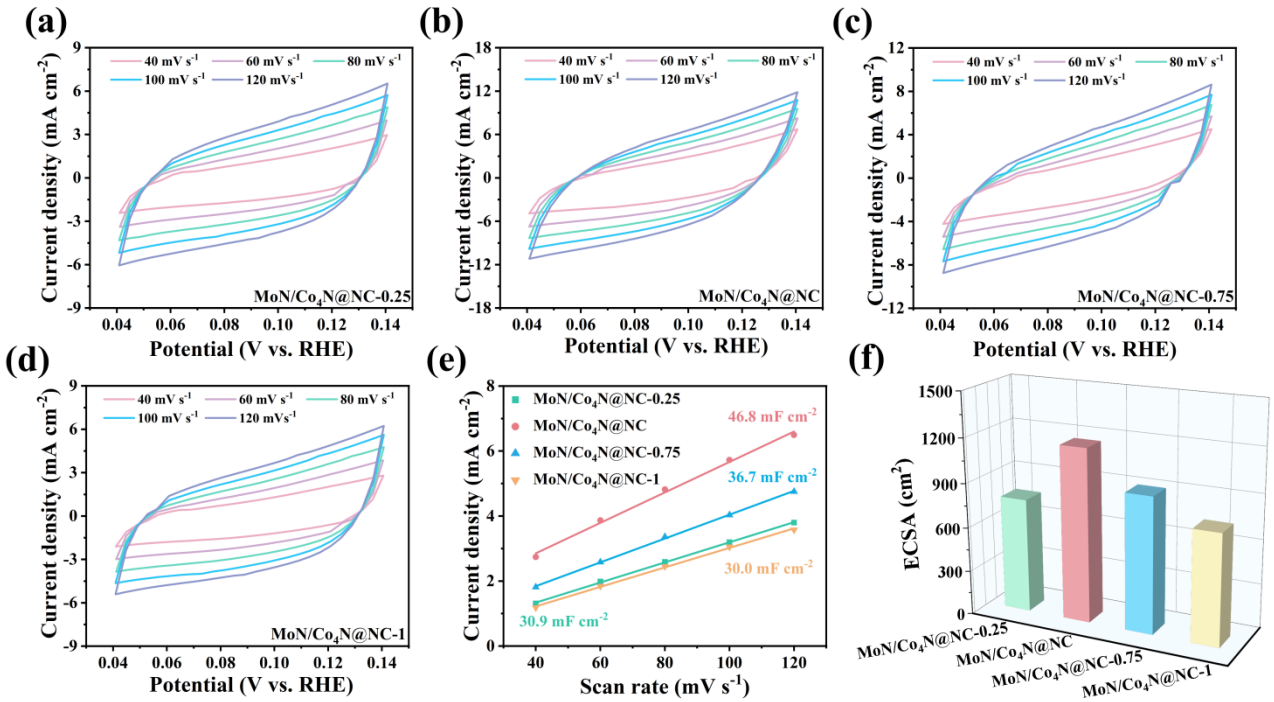

Figure S16. CV curves of (a) MoN/Co_4N@NC-0.25, (b) MoN/Co_4N@NC, (c) MoN/Co_4N@NC-0.75 and (d) MoN/Co_4N@NC-1 in the potential range of 0.04~0.14 V *vs.* RHE at various CV scan rates (40~120 mV s^{-1}) in 1.0 M KOH. (e) C_{dl} values. (f) ECSA values.

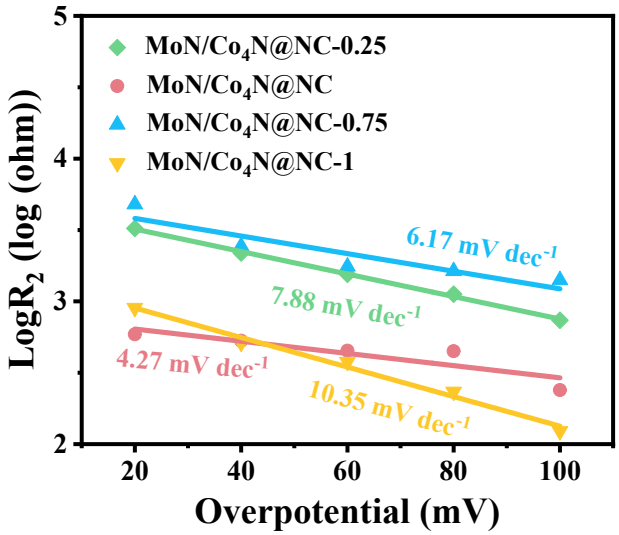

123

124 **Figure S17.** Tafel slopes from EIS of $logR_2$ for catalysts.

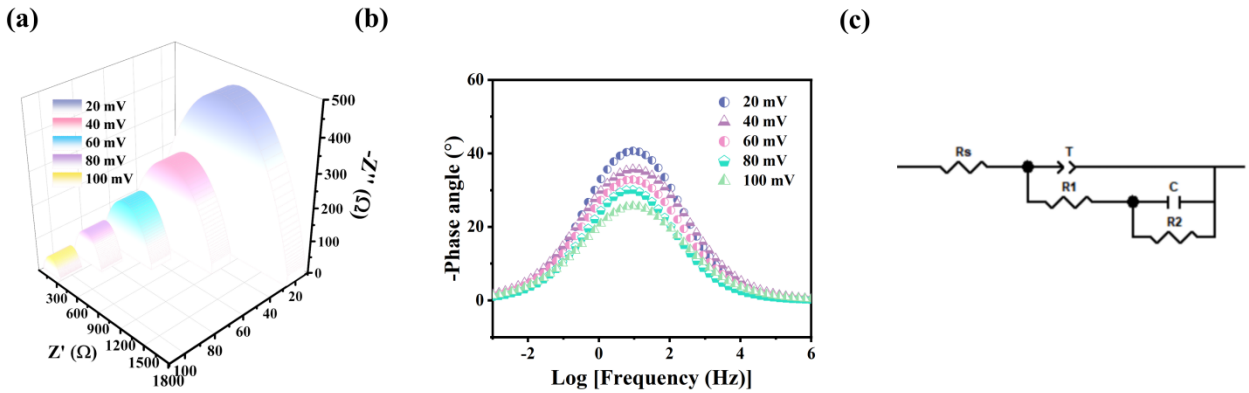

Figure S18. (a) In-situ EIS of MoN/Co_4N@NC-0.25. (b) Bode plot of MoN/Co_4N@NC-0.25. (c) Equivalent circuit model of in-situ EIS.

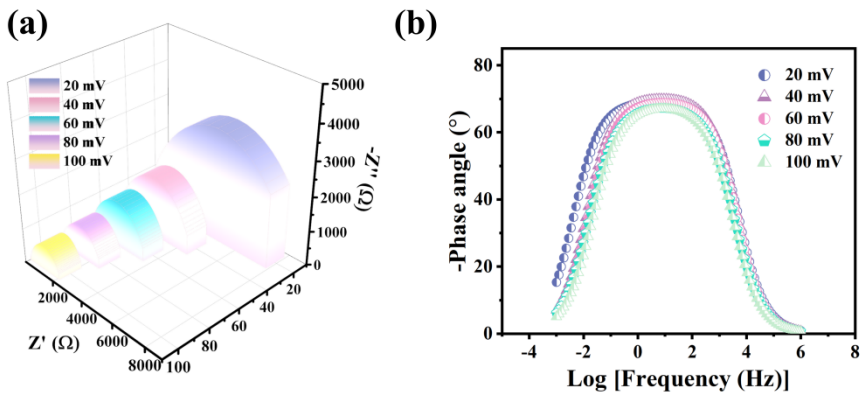

128

129 **Figure S19.** (a) In-situ EIS of MoN/Co_4N@NC-0.75. (b) Bode plot of MoN/Co_4N@NC-0.75.

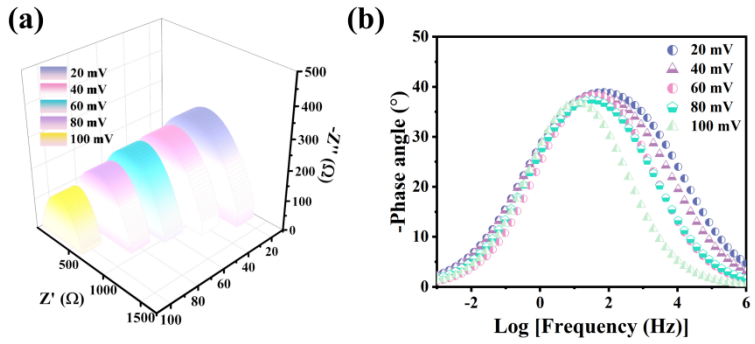

130

131 **Figure S20.** (a) In-situ EIS of MoN/Co_4N@NC-1. (b) Bode plot of MoN/Co_4N@NC-1.

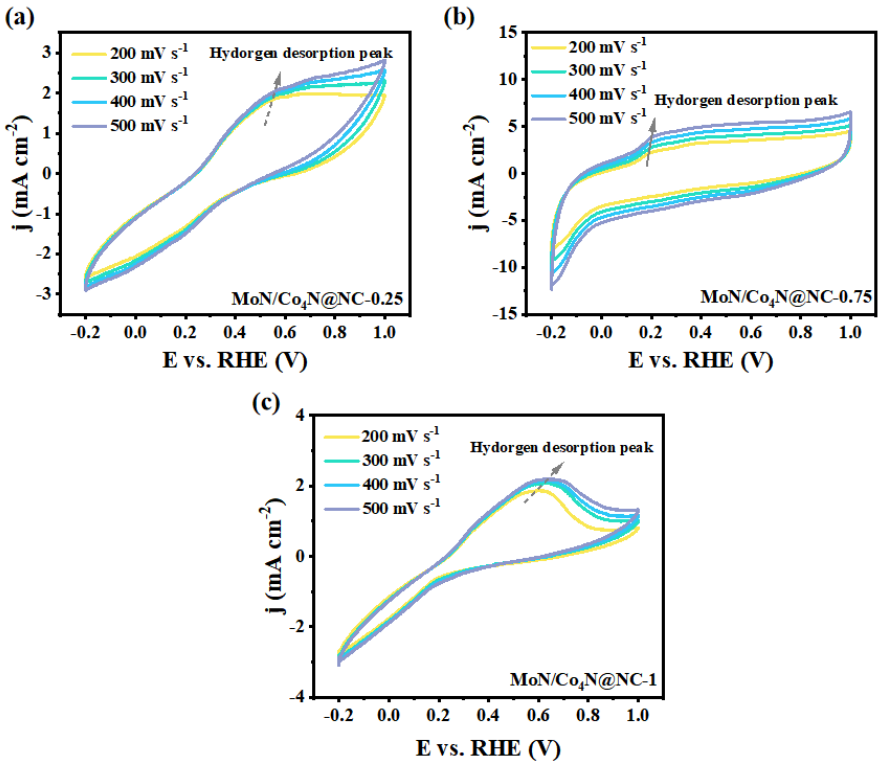

Figure S21. CV curves recorded at various scan rates under Ar.

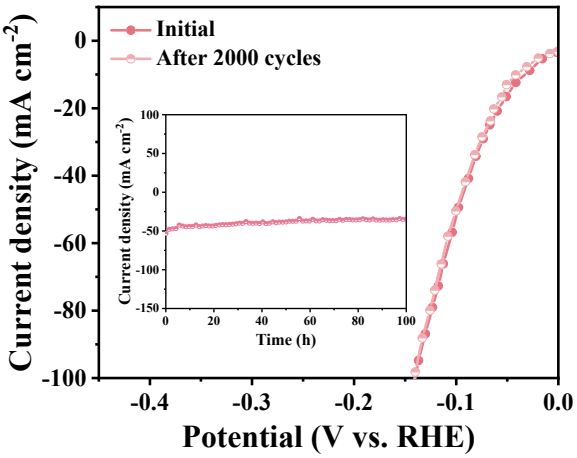

Figure S22. Electrochemical stability of the MoN/Co_4N@NC electrode.

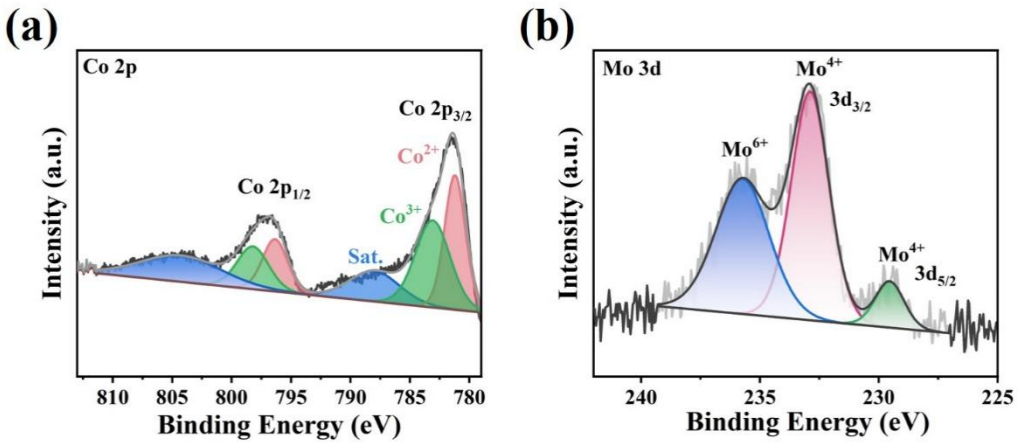

136

137 **Figure S23.** High-resolution XPS spectra for (a) Co 2p and (b) Mo 3d after stability test in 1 M

138 KOH solution.

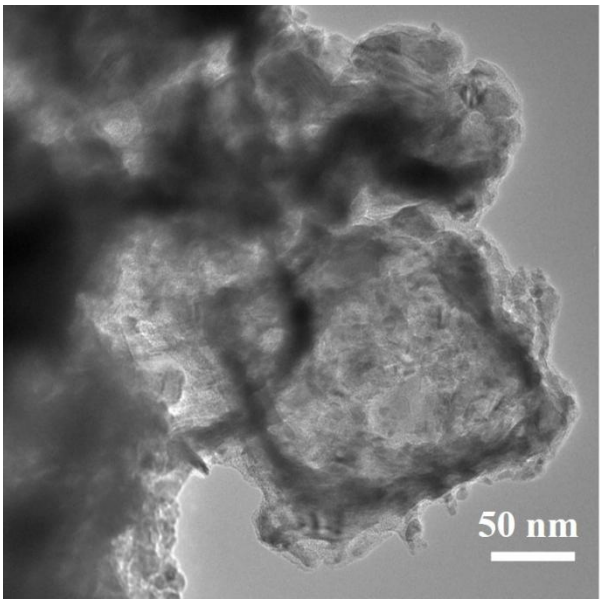

Figure S24. TEM image of MoN/Co_4N@NC after stability test in 1 M KOH solution.

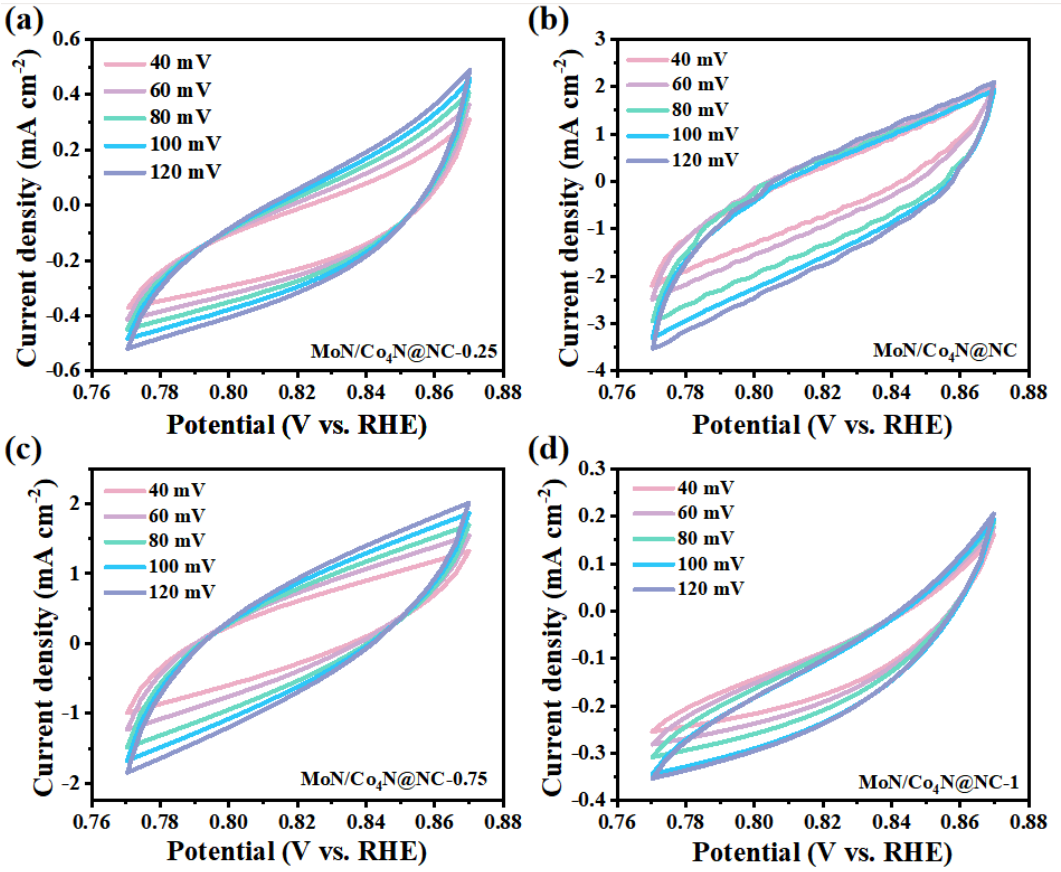

141

142 **Figure S25.** CV curves of (a) MoN/Co_4N@NC-0.25, (b) MoN/Co_4N@NC, (c) MoN/Co_4N@NC-

143 0.75 and (d) MoN/Co_4N@NC-1 in the potential range of 0.77~0.87 V *vs.* RHE at various CV scan

144 rates (40~120 mV s^{-1}) in 1.0 M KOH for OER.

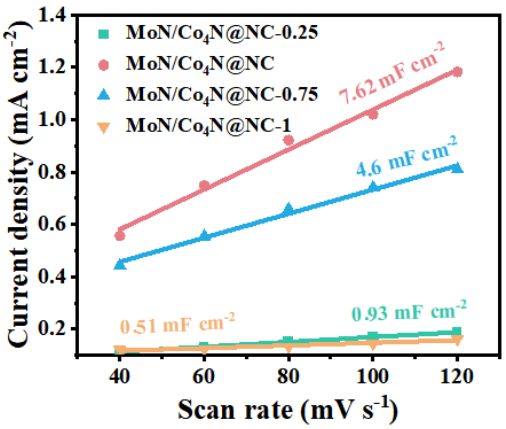

145

146 **Figure S26.** C_{dl} values of MoN/Co_4N@NC-0.25, MoN/Co_4N@NC, MoN/Co_4N@NC-0.75 and

147 MoN/Co_4N@NC-1 in 1.0 M KOH for OER.

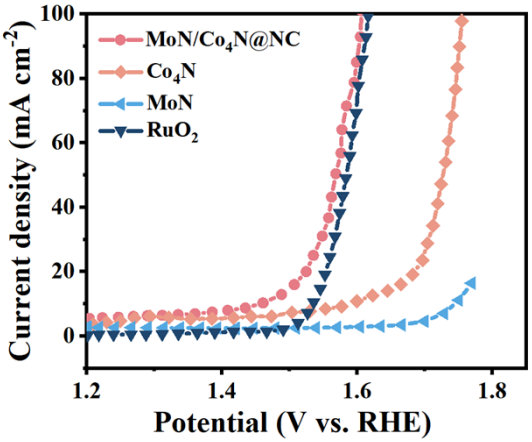

Figure S27. LSV curves of MoN@NC, Co_4N@NC, MoN/Co_4N@NC and RuO_2 in 1.0 M KOH for OER.

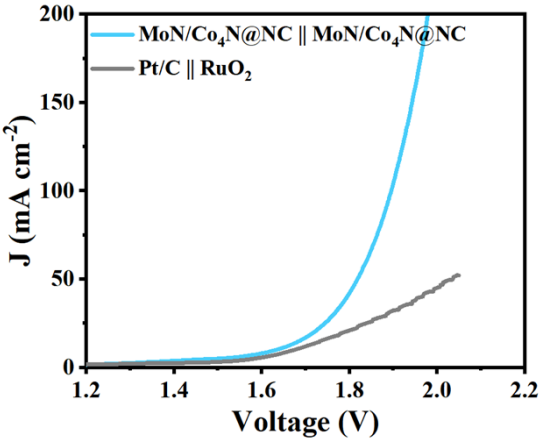

Figure S28. LSV curves of MoN/Co_4N@NC in overall water splitting progress.

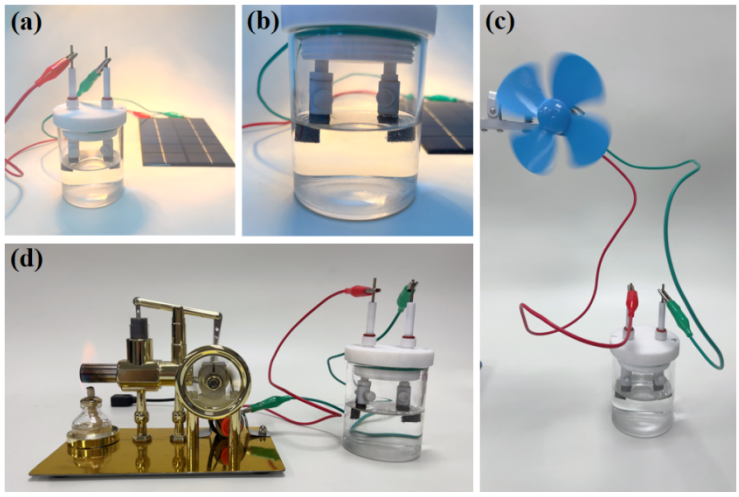

Figure S29. The MoN/Co_4N@NC || MoN/Co_4N@NC electrolyzer of overall water splitting driven by (a,b) solar energy, (c) wind energy and (d) thermal energy.

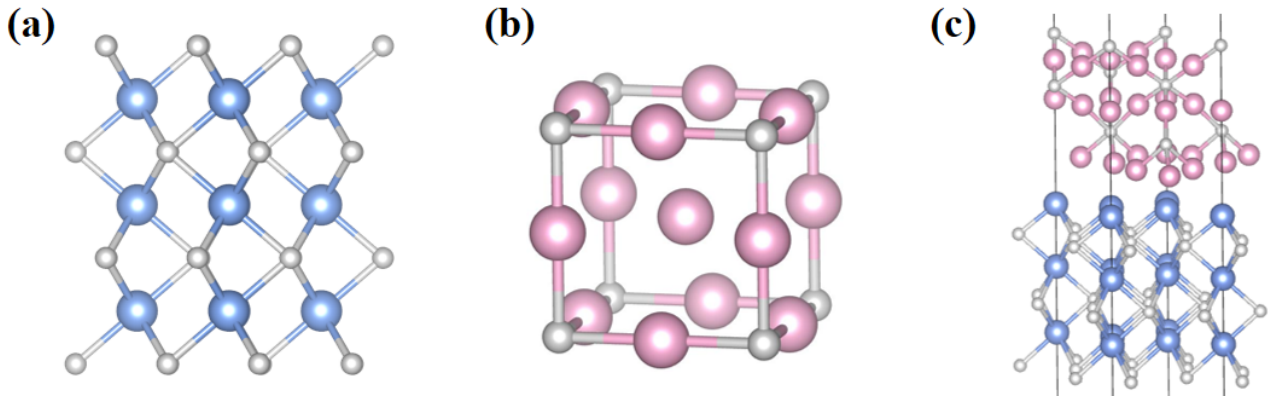

Figure S30. Modeled diagrams of (a) the MoN (111) plane, (b) the Co_4N (111) plane and (c) the MoN (111) / Co_4N (111).

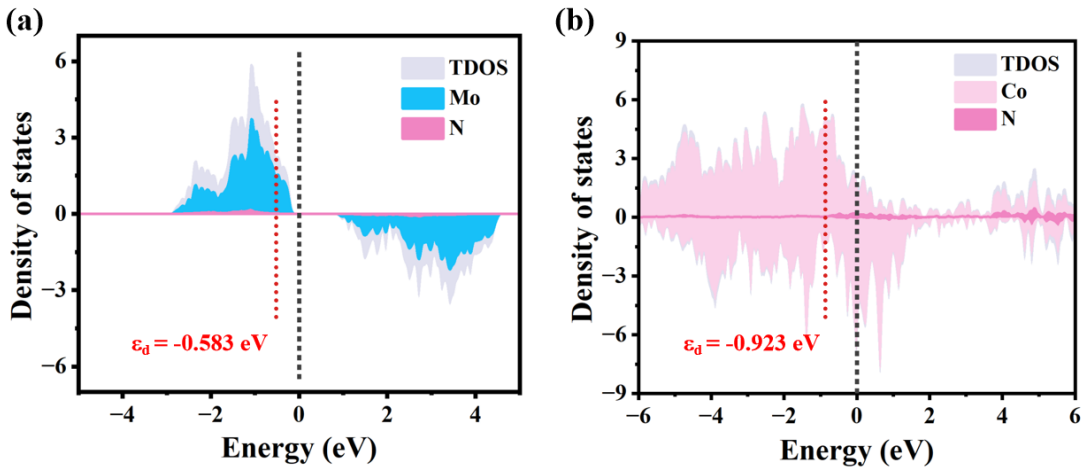

Figure S31. DOS spectra and corresponding d-band centers.

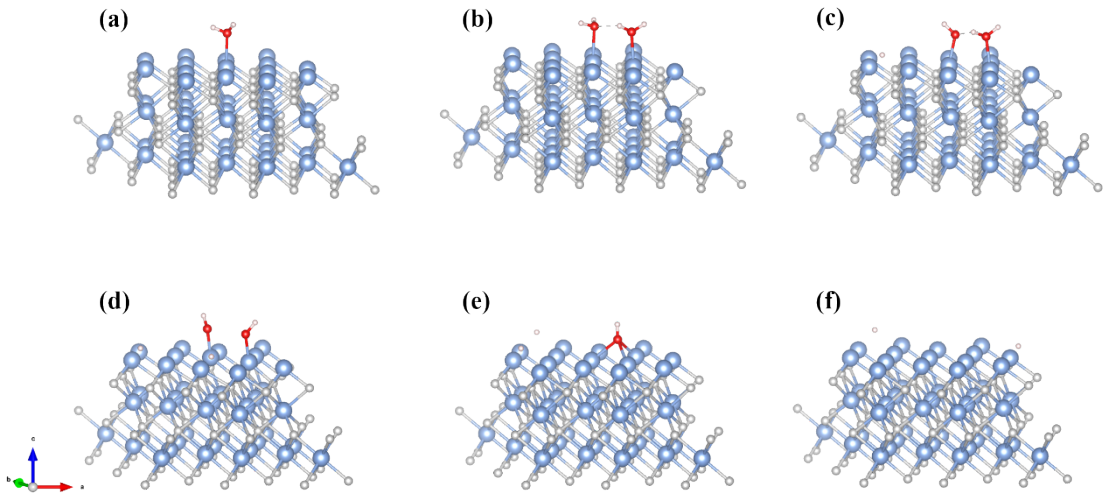

Fig. S32. The most stable geometric configuration of adsorption structure on MoN surface (a) *H_2O; (b) 2*H_2O; (c) *H+*OH+*H_2O; (d) 2*H+2*OH; (e) 2*H+*OH; (f) 2*H.

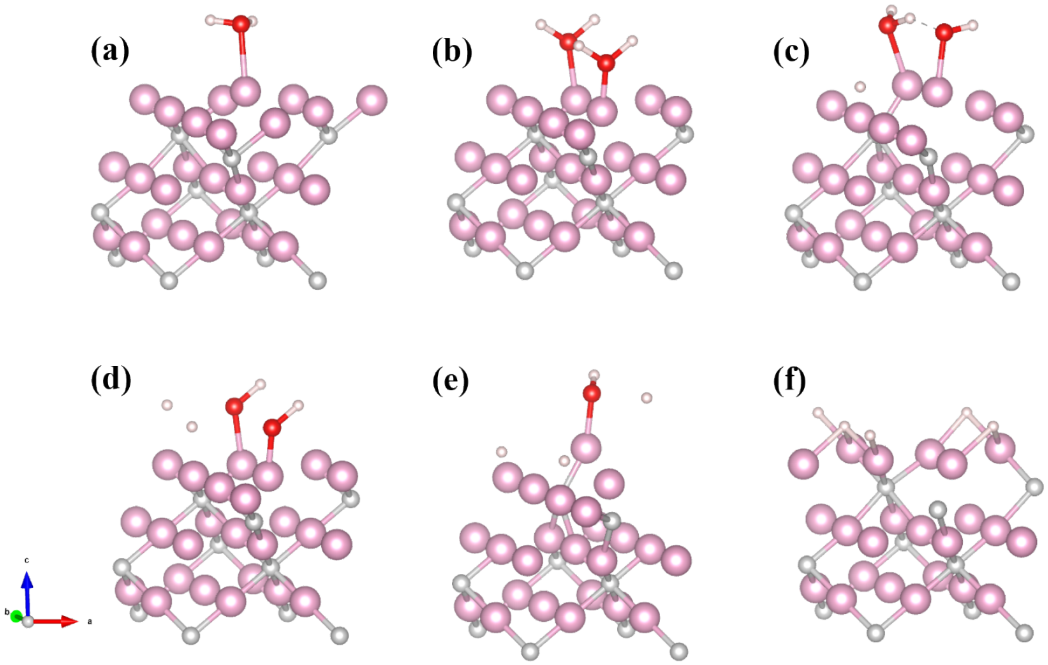

165

166 **Fig. S33.** The most stable geometric configuration of adsorption structure on Co_4N surface (a) $*H_2O$;

167 (b) $2*H_2O$; (c) $*H+*OH+*H_2O$; (d) $2*H+2*OH$; (e) $2*H+*OH$; (f) 2*H.

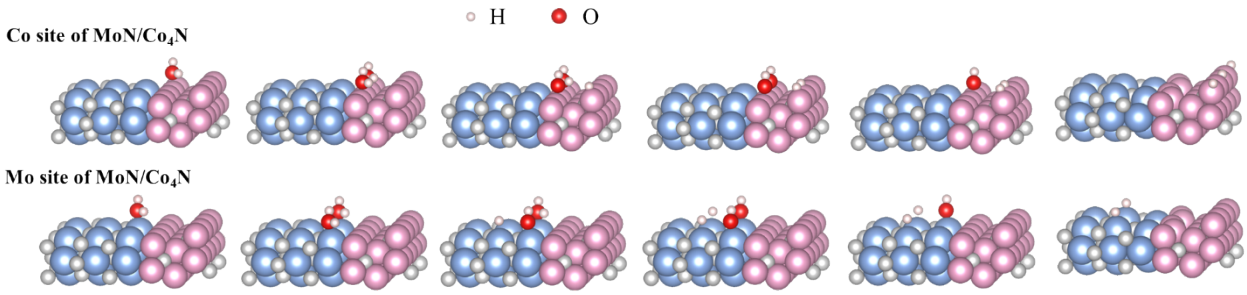

168

169 **Fig. S34.** Schematic diagrams illustrate each step of the alkaline hydrogen reaction process for the

170 Co site of MoN/Co_4N and the Mo site of MoN/Co_4N, respectively.

Table S1. Relative content of elements in prepared samples.

Catalyst	C (%)	N (%)	O (%)	Co (%)	Mo (%)	Co/Mo
Co_4N@NC	39.63	5.03	42.24	13.11	0	/
MoN/Co_4N@NC-0.25	33.01	20.63	32.28	7.18	6.91	1.04
MoN/Co_4N@NC	19.29	39.45	20.51	7.11	13.65	0.52
MoN/Co_4N@NC-0.75	19.69	41.42	19.96	5.65	13.28	0.425
MoN/Co_4N@NC-1	17.28	42.46	20.69	4.75	14.81	0.32

Table S2. Values of Tafel, R_{ct} and overpotential at 10 mA cm^{-2} for prepared samples in HER.

Catalyst	η (mV) @ 10 mA cm^{-2}	Tafel mV dec^{-1}	Rct (Ω)
MoN/Co_4N@NC	29	55.8	19.1
MoN@NC	180	93.4	490.5
Co_4N@NC	159	83	168.6
MoN/Co_4N@NC-0.25	75	89	82.4
MoN/Co_4N@NC-0.75	55	73.7	56.9
MoN/Co_4N@NC-1	85	107.9	113.9

Table S3. Comparison of overall water splitting activity of MoN/Co_4N@NC with other transition metal-based electrocatalysts.

Electrocatalyst	*Electrolyte*	*J / mA cm^{-2}*	*Cell voltage*	*References*
MoN/Co_4N@NC	1.0 M KOH	10	1.63V	This work
$NiCo_2N$/NF	1.0 M KOH	10	1.70V	*ChemSusChem*, 2017, 10, 4170.
Mo-NiCoP/NiCoN FS	1.0 M KOH	10	1.68V	*FlatChem*, 2023, 42, 100552
Co/VN/NC-8	1.0 M KOH	10	1.74V	*ACS Appl. Nano Mater.*, 2025, 8, 14, 7026-7038.
Fe_3N@CN-700	1.0 M KOH	10	1.64V	*Sustain Energ Fuels*, 2024, 8, 3452-3464.
Co_4N@Fe/N-C-18h	1.0 M KOH	10	1.758V	*Carbon Energ.*, 2024, 6, e505.
V-CoN/CoN-1-400	1.0 M KOH	10	1.69V	*J. Solid State Chem.*, 2024, 335, 124701.
Ni/MoN@NCNT/CC	1.0 M KOH	10	1.699V	*ChemElectroChem*, 2020, 7, 745.
CoO/Co_4N/NF	1.0 M KOH	10	1.79V	*J. Mater. Chem. A*, 2018,6, 24767-24772.
Fe-CoP nanoFC	1.0 M KOH	10	1.671V	*Int. J. Hydrogen Energy*, 2024, 90, 1401-1410.
Ce_1-CoP	1.0 M KOH	10	1.65V	*ACS Sustainable Chem. Eng.*, 2020, 8, 27, 10009-10016.
CoP@a-CoO_x	1.0 M KOH	10	1.66V	*Adv. Sci.*, 2018, 5, 1800514.

References

[1] M. Huang, S. Zhou, D.-D. Ma, W. Wei, Q.-L. Zhu, Z. Huang, Chem. Eng. J. 2023, 473, 145170.

[2] J. P. Perdew, K. Burke, M. Ernzerhof, Phys. Rev. Lett. 1996, 77, 3865.

[3] G. Kresse, D. Joubert, Phys. Rev. B 1999, 59, 1758.

[4] J. P. Perdew, K. Burke, M. Ernzerhof, Generalized Gradient Approximation Made Simple, Phy. Rev. Lett. 77 (1996) 3865.

[5] H. J. Monkhorst, J. D. Pack, Phys. Rev. B 1976, 13, 5188.